1 Rapid Compression Machine

1.1 Experimental Procedure

The studies in this dissertation were conducted using the Rapid Compression Machine (RCM) constructed by Mittal around 2005 and described in the work of Mittal and Sung [1] and Mittal [2]. This RCM has been used to study the autoignition behavior of a number of fuels, including *n*-decane, methylcyclohexane, hydrogen, syngas, dimethyl ether, methanol, toluene, benzene, di-isobutylene, iso-octane, jet fuel, and gasoline [3–18], in addition to the studies presented in this work.

A modern RCM operates by rapidly compressing (hence the name) a test gas mixture to targeted pressure and temperature conditions. The compression is effected by either a single piston or dual, opposed pistons. Upon reaching the targeted state, the piston (or pistons) is stopped and fixed in place so that the reactions proceed in a constant volume reactor. When studying autoignition with an RCM, the primary data are the measured pressure traces during and after the compression stroke. These pressure traces are processed to derive information such as the pressure and temperature at the end of compression (EOC) and the ignition delay. It is also possible to employ laser diagnostics or extract gas samples from the reactor to examine reaction pathways in more detail.

The present RCM is a pneumatically-driven/hydraulically-stopped single-piston arrangement. A schematic of the RCM is shown in **??**. The RCM consists of four chambers and three pistons that are used to control machine. The chambers are called the reaction chamber, the hydraulic chamber, the pneumatic chamber, and the driving tank; similarly, the pistons are called the reactor, hydraulic, and pneumatic pistons and are each installed in the chamber of the same name. The rear of the reaction chamber is bolted to the front of the hydraulic chamber; seals in the face of the hydraulic chamber prevent oil from leaking and contaminating the reaction chamber. The driving tank and the rear of the pneumatic chamber are connected by a union; a seal around the circumference of the pneumatic piston seals gas in the driving tank from the front of the pneumatic chamber. Thus, the pneumatic piston can be driven by pressure from the driving tank on its rear and pressure from the

pneumatic chamber on its front. The three pistons are connected by a rod running from the front of the pneumatic piston to the rear of the reactor piston so that they move as one; this will be referred to as the piston assembly.

At the start of an experimental run, with the piston in the EOC position, the reaction chamber is vacuumed to less than one Torr. Next, the piston assembly is retracted by pressurizing the front face of the piston in the pneumatic chamber. For safety, and to prevent damage to the RCM, the driving tank should be filled to limit the acceleration of the piston assembly during this retraction. The pressure on the front of the pneumatic piston pulls the piston assembly rearward and seats the rear of the hydraulic piston onto an O-ring in the rear of the hydraulic chamber. The hydraulic chamber is filled with oil to a pressure of approximately 800 psi, providing a rearward force on the front face of the hydraulic piston. Then, the air pressure is released from the front of the pneumatic chamber and the driving tank is filled to the desired driving pressure. The force on the hydraulic piston opposes the force on the pneumatic piston from the driving tank and the piston assembly remains at rest. Then, the reaction chamber is filled with the required initial pressure of test gas mixture from the mixing tank. Finally, compression is triggered by releasing the hydraulic pressure through an electrically-operated solenoid valve. The piston assembly is driven forward by the unbalanced force from the pressure in the driving tank on the pneumatic piston. The gases in the reaction chamber are brought to the compressed pressure (P_C) and compressed temperature (T_C) conditions in approximately 30–50 ms.

The required driving pressure for a given EOC pressure can be estimated from a force balance between the force on the pneumatic piston from the driving tank and the force on the reactor piston from the test gases, as shown in Eq. (1c).

$$P_{d,\min} A_p = P_{r,\mathrm{EOC}} A_r \tag{1a}$$

$$P_{d,\min} \frac{\pi d_p^2}{4} = P_{r,\mathrm{EOC}} \frac{\pi d_r^2}{4} \tag{1b}$$

$$P_{d,\min} = P_{r,\mathrm{EOC}} \frac{d_r^2}{d_p^2} \tag{1c}$$

In Eq. (1), $P_{d,\min}$ is the minimum driving pressure, A_p is the cross-sectional area of the pneumatic piston, $P_{r,\mathrm{EOC}}$ is the pressure in the reactor at the EOC (i.e. P_C), A_r is the cross-sectional area of the reactor piston, d_p is the diameter of the pneumatic piston, and d_r is the diameter of the reactor piston.

The minimum driving pressure is such that the piston does not rebound at the EOC due to pressure on the reactor piston. So that the driving pressure can be much lower than the EOC pressure, the diameter ratio of the reactor piston to the driver piston is $2/5$, allowing a factor of 6.25 lower driving pressure than EOC pressure. The actual driving pressure should exceed the minimum by some safety margin so that the reactor remains at constant volume even if there is some pressure rise due to heat release in the reaction chamber prior to the main ignition.

There is not a theoretical upper limit on the driving pressure. It is desired that the piston should reach the EOC conditions in as short a time as possible to minimize heat loss from the reactants to the reactor walls and minimize the time for reactions to occur during the compression stroke. This implies that the driving pressure should be made as high as possible so that the highest piston velocity is achieved. However, higher piston velocities require a higher deceleration at the EOC. In the present RCM, the deceleration is provided by venting the hydraulic oil between steps on the hydraulic piston and matched steps on the front of the hydraulic chamber. If the piston is overdriven—that is, the driving pressure is too high—the piston will not be sufficiently decelerated by the oil venting and will impact the front of the hydraulic chamber at high velocity. This can damage the RCM and cause the piston to rebound elastically. It also generates substantial noise in the pressure trace and should be avoided.

Typical driving gas pressures are between 50 psi for $P_C = 15$ bar experiments to 125 psi for $P_C = 50$ bar experiments. These driving pressures represent a good compromise between the minimum required for no rebound at EOC due to pressure and no rebound at EOC due to elastic reaction. Nonetheless, a small amount of piston rebound can be expected during/after the main ignition event. This small rebound may have an effect on the computation of ignition delay if it reduces the pressure rise rate during the ignition; it is expected that this effect will be very small relative to the typical random uncertainty in ignition delay experiments. Moreover, the driving pressures required to balance the full pressure rise during to ignition are more likely cause elastic rebound, especially for high P_C when the post-ignition pressure rise is greater.

The EOC conditions (P_C and T_C) can be independently varied. This is made possible by independent variation of the compression ratio, initial pressure and initial temperature, and the specific heat ratio of the test gases. The compression ratio can be increased by adding spacers onto the rear of the hydraulic chamber, increasing the stroke, and can be reduced by adding split shims onto the rear of the reaction chamber, increasing the EOC clearance length.

1.2 Test Gas Mixture Preparation

Fuel/oxidizer pre-mixtures are prepared in two mixing tanks, one approximately 17 L and the other approximately 15 L in volume. These large volumes allow many runs to be conducted from one mixture preparation. The mixing tanks are connected to the reaction chamber by flexible stainless steel manifold tubing. The tanks, reaction chamber, and connecting manifold are wrapped in heating tape and insulation to control the initial temperature of the mixture. Temperature controllers from Omega Engineering use thermocouples placed on the lid of each mixing tank, approximately in the center of each mixing tank, embedded in the wall of the reaction chamber, and near the inlet valve of the reaction chamber to control the preheat temperature of the mixture. A static pressure transducer measures the pressure in the manifold and mixing tanks. This transducer is used during mixture preparation and to measure the initial pressure of a given experiment. Two transducers are for various experiments in this work, as described below in Sec. 1.8.

Most of the fuels studied in this work are liquids at room temperature and pressure and have relatively low vapor pressure. A similar procedure, outlined below, was used for all of the butanol isomers, *iso*-pentanol, and methylcyclohexane. First, the mixing tanks are vacuumed to an ultimate pressure less than 5 Torr. The liquid fuel is massed in a syringe to a precision of 0.01 g prior to injection through a septum. Proportions of O_2, N_2, and Ar are added manometrically at room temperature. The preheat temperature of the RCM is set above the saturation point for each fuel to ensure complete vaporization. The vapor pressure as a function of temperature is calculated according to fits taken from Yaws [19]. A magnetic stirrer mixes the reactants. The temperature inside the mixing tank is allowed to equilibrate for approximately 1.5 h.

This approach to mixture preparation has been validated in several previous studies by withdrawing gas samples from the mixing tank and analyzing the contents by GC/MS [20], GC-FID [3], and GC-TCD [7]. These studies have verified the concentration of *n*-butanol, *n*-decane, and water, respectively. In addition, both the work by Kumar et al. [3] on *n*-decane and the study of Weber et al. [20] on *n*-butanol confirmed that there was no fuel decomposition over the course of a typical set of experiments. Furthermore, within this study, each new mixture preparation is checked against previously tested conditions to ensure reproducibility.

1.3 Definition of Ignition Delay

The pressure in the reaction chamber during an experiment is monitored by a Kistler 6125B piezoelectric dynamic pressure transducer. The charge signal from the transducer is amplified and converted to a voltage by a Kistler 5010B charge amplifier. The voltage is sent to a National Instruments cDAQ equipped with the NI-9215 module. The signal is recorded by a LabView VirtualInstrument at 50 kHz.

Figure 1 shows a representative pressure trace from these experiments with methylcyclohexane (MCH) at $P_C = 50$ bar, $T_C = 761$ K, and $\phi = 1.5$ (See **??**). Note that Fig. 1 shows a case with two stages of ignition; not all of the fuels studied had conditions that showed two-stage ignition. Nonetheless, the ignition delay is consistently defined in all the work in this study. The definitions

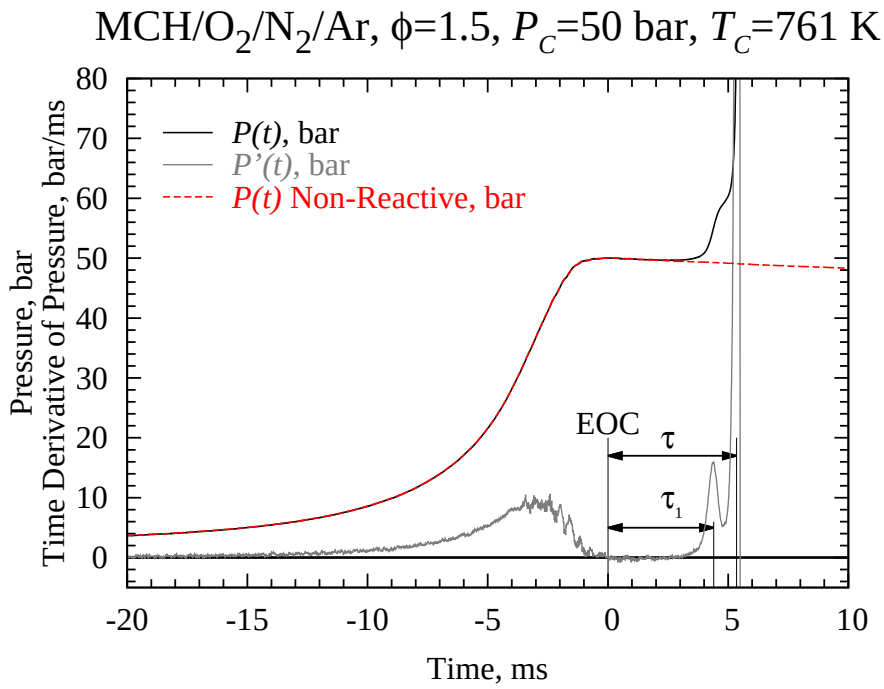

Figure 1: Representative pressure trace indicating the definition of the first stage and overall ignition delays and the corresponding non-reactive pressure trace. EOC stands for End of Compression.

of the EOC and the ignition delays are indicated on the figure. The end of compression time is defined as the time when the pressure reaches its maximum before first stage ignition occurs, or for cases where there is no first stage ignition, the maximum pressure before the overall ignition occurs. The first stage ignition delay is the time from the end of compression until the first peak in the time derivative of the pressure. The overall ignition delay is the time from the end of compression until the largest peak in the time derivative of the pressure.

Each unique P_C and T_C condition is repeated at least 5 times to ensure repeatability of the experiments. The experiment closest to the mean of the runs at a particular condition is chosen for analysis and presentation. The standard deviation of all of the runs at a condition is less than 10% of the mean in all cases.

1.4 Non-Reactive Experiments

Figure 1 also shows a non-reactive pressure trace. Due to heat loss from the test mixture to the cold

reactor walls, the pressure and temperature of the gas in the reaction chamber will decrease after the end of compression. A non-reactive pressure trace is measured that corresponds to each unique P_C and T_C condition studied to quantify the effect of the heat loss on the ignition process and to verify that no heat release has occurred during the compression stroke. The non-reactive pressure trace is acquired by replacing the oxygen in the oxidizer with nitrogen, so that the specific heat ratio of the initial mixture is maintained, but the heat release due to exothermic oxidation reactions is eliminated. Maintaining a similar specific heat ratio ensures that the non-reactive experiment faithfully reproduces the conditions of the reactive experiment. A representative non-reactive pressure trace is shown in Fig. 1 corresponding to the experimental conditions in the figure.

1.5 Reaction Chamber Homogeneity

An RCM to be used for studies of homogeneous chemistry—as in this study—must ensure that homogeneous conditions exist inside the reaction chamber for the duration of the experiment. Due to the high piston velocities required to minimize heat loss and reaction during the compression stroke, complex fluid mechanical effects can strongly affect the state of the reactants at the EOC. The most important of these effects is caused by the motion of the piston itself, where the piston pushes the wall boundary layer into a roll-up vortex [21]. This cold vortex mixes with the hotter gases near the center of the reaction chamber and causes large spatial inhomogeneities of temperature and species.

To facilitate spatially homogeneous conditions in the reactor and reduce the effect of the roll-up vortex, it is necessary to trap the boundary layer. This is accomplished on the present RCM by a crevice machined into the crown of the piston, shown in cross-section in **??**. The boundary layer enters the crevice through the converging section as the piston moves forward and is trapped within the crevice. The dimensions of the crevice were optimized by Mittal [2] through CFD simulations for high-pressure conditions. Subsequently, Mittal and Sung [22] experimentally showed that the optimized crevice design provides homogeneous conditions in the reaction chamber up to approximately 150 ms after the EOC. By using PLIF measurements of acetone-seeded mixtures, Mittal

and Sung [22] showed that there was a core region of gases near the center of the reactor whose temperature remained spatially homogeneous.

1.6 Determination of Reactant Temperature

Two independent thermodynamic properties are required to fix the thermodynamic state of the reactants in the reaction chamber at a given time. The first property is the pressure, measured by the dynamic pressure transducer, as discussed previously; the second property is chosen to be the temperature.

In general, it is rather difficult to directly measure the temperature of the gases in the reaction chamber during and after compression. Intrusive methods such as thermocouples may introduce inhomogeneities into the reaction chamber and non-intrusive optical techniques are difficult to set up and require extensive calibration at the pressures of interest in RCM studies. Thus, the temperature is determined indirectly by applying an assumption called the "adiabatic core hypothesis" to the reaction chamber [1, 21].

If all of the gases in the reaction chamber were compressed isentropically, the temperature at the end of compression could be found by the following relations:

$$\ln(\mathrm{CR}) = \int_{T_0}^{T_{ic}} \frac{1}{T\,(\gamma - 1)}\,\mathrm{d}T \tag{2a}$$

$$\ln\left(\frac{P_{ic}}{P_0}\right) = \int_{T_0}^{T_{ic}} \frac{\gamma}{T\,(\gamma - 1)}\,\mathrm{d}T \tag{2b}$$

where CR is the volumetric compression ratio, T_0 is the initial temperature, T_{ic} is the temperature at the end of isentropic compression, γ is the temperature-dependent ratio of specific heats, P_{ic} is the pressure at the end of isentropic compression, and P_0 is the initial pressure.

However, experiments show that the measured pressure in the reaction chamber does not reach the value of P_{ic} calculated by using the geometric compression ratio. The difference is due to finite heat loss from the reactants to the reactor walls and the crevice volume during the compression. Under the adiabatic core hypothesis, it is assumed that the heat loss from the reactants only occurs

in a thin boundary layer near the wall, and the central core region is unaffected by heat loss (i.e. the core is adiabatic) [23]. Thus, the heat loss is modeled as an effective reduction in the compression ratio, and the temperature during the compression stroke can be calculated by:

$$\ln\left(\frac{P_C}{P_0}\right) = \int_{T_0}^{T_C} \frac{\gamma}{T\,(\gamma - 1)}\,\mathrm{d}T \tag{3}$$

where P_C is the measured pressure at the end of compression, T_C is the temperature at the end of compression, and the other variables are the same as in Eq. (2).

After the end of compression, the pressure in the reaction chamber decreases, as can be seen in Fig. 1. This pressure decrease is caused by heat loss from the reactants in the constant volume reaction chamber and is accompanied by a decrease in the temperature of the reactants. To model the thermodynamic state after the end of compression, the adiabatic core hypothesis is applied, and the heat loss is assumed to occur only in a thin boundary layer near the reactor walls. Thus, the core region is modeled as adiabatic, and the heat loss from the boundary layer can be modeled as an isentropic volume expansion.

1.7 Determination of Compressed Temperature

In general, the specific heat ratio used in Eqs. (2) and (3) is an unknown function of temperature and composition, so Eq. (3) cannot be integrated directly to find T_C. If the specific heats are parameterized with a linear fit and the composition is assumed to be fixed, it is possible to integrate Eq. (3) directly, but this process is quite tedious; nonetheless, it will be applied in Sec. 1.8 to determine the uncertainty of T_C. In general, the simplest method of calculating T_C is to use software to numerically integrate Eq. (3).

In this work, the CHEMKIN-Pro [24] software is used to perform the numerical integration and calculation of T_C. The CHEMKIN-Pro software provides the facility for a user-specified volume as a function of time to be applied to a homogeneous, adiabatic reactor. Since the adiabatic core of the reaction chamber is modeled as undergoing an isentropic volumetric compression followed

by an isentropic volumetric expansion, the user-specified volume functionality is used to compute the RCM reactor state as a function of time. A volume trace for simulation is computed from the measured pressure trace using the isentropic relation:

$$\frac{V_2}{V_1} = \left[\frac{P_1}{P_2}\right]^{\frac{1}{\gamma}} \tag{4}$$

where V_1 and V_2 are the volumes at consecutive time points, P_1 and P_2 are the pressures at consecutive time points, and γ is the temperature dependent specific heat. This equation is applied during and after the compression stroke to calculate the volume trace. In Eq. (4) it is assumed that changes in composition of the reactants are negligible during the compression stroke.

For use in Eq. (4), γ is tabulated for each time point. Thus, the temperature at each time point must also be computed by using the isentropic relation for temperature:

$$\frac{T_2}{T_1} = \left[\frac{P_2}{P_1}\right]^{\frac{\gamma-1}{\gamma}} \tag{5}$$

where T_2 and T_1 are the temperatures at consecutive time points. Since T_2 depends on the value of γ, which in turn depends on T_2, Eq. (5) is iterated until the temperature changes by less than one tenth of one percent on consecutive iterations. Once again, it is assumed that changes in composition have a negligible influence on the ratio of specific heats. The temperature calculated by Eq. (5) is typically within 1K of the temperature calculated by CHEMKIN-Pro.

1.8 Uncertainty of Ignition Delay and Compressed Temperature

The uncertainty of the compressed temperature is an important parameter to report. Since T_C is not measured, we must perform an uncertainty propagation analysis on the equation used to calculate T_C, Eq. (3). First, we simplify the term involving γ in Eq. (3). By definition, γ is the ratio of the

specific heat at constant pressure to that at constant volume

$$\gamma = \frac{C_p}{C_v} = \frac{C_p/R}{C_v/R} \tag{6}$$

where C_p and C_v are the specific heats in molar units at constant pressure and volume, respectively, and R is the universal gas constant, used to produce non-dimensional specific heats. Letting a hat denote the non-dimensional specific heats, the difference between the non-dimensional specific heats is one, $\hat{C}_v = \hat{C}_p - 1$. Then, it follows that

$$\frac{\gamma}{\gamma - 1} = \frac{\frac{\hat{C}_p}{\hat{C}_v}}{\frac{\hat{C}_p}{\hat{C}_v} - 1} = \frac{\frac{\hat{C}_p}{\hat{C}_p - 1}}{\frac{\hat{C}_p}{\hat{C}_p - 1} - 1} = \frac{\frac{\hat{C}_p}{\hat{C}_p - 1}}{\frac{1}{\hat{C}_p - 1}} = \hat{C}_p \tag{7}$$

In Eq. (3), the mean specific heat ratio for the mixture should be used; thus, the simplification as shown in Eq. (7) requires that the specific heat $\hat{C}_p$ also be the mean specific heat. In the following, we assume that there is negligible change of the mean specific heat due to changes in reactant mole fractions. The mean specific heat is simply the sum of the product of the species mole fractions and their specific heats

$$C_{p,\text{total}} = \sum_i X_i C_{p,i} \tag{8a}$$

$$\hat{C}_{p,\text{total}} = \frac{\sum_i X_i C_{p,i}}{R} \tag{8b}$$

where i indicates the species and X_i is the species mole fraction. In the NASA polynomial formulation used by CHEMKIN, the non-dimensional specific heat at constant pressure as a function of temperature is represented by a fourth-order polynomial fit

$$\hat{C}_{p,i} = c_{1,i} + c_{2,i}T + c_{3,i}T^2 + c_{4,i}T^3 + c_{5,i}T^4 \tag{9}$$

In general, this means that the specific heat can be non-linear. However, since the mixtures prepared

in this study are composed primarily of O_2, N_2 and Ar (i.e. no more than 7% of any mixture is the fuel), and since the specific heats of O_2, N_2 and Ar are only weakly temperature dependent over the range of temperatures experienced during compression, we will approximate the total specific heat as a linear function of temperature.

$$\begin{aligned}\hat{C}_{p,\text{total}} &= \sum_i X_i \hat{C}_{p,i} \\ &= \sum_i X_i \left(\sum_{j=1}^{5} c_{j,i} T^{j-1} \right) \\ &\approx a + bT\end{aligned} \tag{10}$$

a and b are found by fitting the total non-dimensional specific heat over the temperature range from 300–1100 K, as discussed below in Sec. 1.8.4.

With this approximation of the specific heat, we can integrate Eq. (3) to find the compressed temperature

$$\ln \frac{P_C}{P_0} = \int_{T_0}^{T_C} \frac{\gamma}{T(\gamma - 1)} \, \mathrm{d}T = \int_{T_0}^{T_C} \frac{\hat{C}_p}{T} \, \mathrm{d}T \tag{11a}$$

$$= \int_{T_0}^{T_C} \frac{a + bT}{T} \, \mathrm{d}T \tag{11b}$$

$$= a \ln T + bT \Big|_{T_0}^{T_C} \tag{11c}$$

$$\ln \frac{P_C}{P_0} = a \ln T_C + b \ln T_C - (a \ln T_0 + bT_0) \tag{11d}$$

Solving Eq. (11d) for T_C

$$T_C = \frac{aW\left(\frac{b}{a} \exp\left[\frac{bT_0}{a} \right] T_0 \left[\frac{P_C}{P_0} \right]^{\frac{1}{a}} \right)}{b} \tag{12}$$

where $W(...)$ is Lambert's W function [25]. With an explicit function for T_C, we can estimate the uncertainty in T_C by the root square sum of the uncertainty in the parameters in Eq. (12) [26]. The

parameters are P_C, P_0, T_0, a, and b.

$$U_{T_C} = \sqrt{\left(\frac{\partial T_C}{\partial P_C} U_{P_C}\right)^2 + \left(\frac{\partial T_C}{\partial P_0} U_{P_0}\right)^2 + \left(\frac{\partial T_C}{\partial T_0} U_{T_0}\right)^2 + \left(\frac{\partial T_C}{\partial a} U_a\right)^2 + \left(\frac{\partial T_C}{\partial b} U_b\right)^2} \tag{13}$$

Then, letting

$$D = W\left(\frac{b}{a}\exp\left[\frac{bT_0}{a}\right]T_0\left[\frac{P_C}{P_0}\right]^{\frac{1}{a}}\right)$$

the partial derivatives of Eq. (12) with respect to the parameters are

$$\frac{\partial T_C}{\partial P_C} = \frac{D}{bP_C\,(D+1)} \tag{14a}$$

$$\frac{\partial T_C}{\partial P_0} = \frac{-D}{bP_0\,(D+1)} \tag{14b}$$

$$\frac{\partial T_C}{\partial T_0} = \frac{(a+bT_0)\,D}{bT_0\,(D+1)} \tag{14c}$$

$$\frac{\partial T_C}{\partial a} = \frac{-D\left[bT_0 + \ln\left(P_C/P_0\right) - aD\right]}{ab\,(D+1)} \tag{14d}$$

$$\frac{\partial T_C}{\partial b} = \frac{D\,(bT_0 - aD)}{b^2\,(D+1)} \tag{14e}$$

The uncertainties of the parameters, U_j in Eq. (13), are in general found by their own root square sum procedure

$$U_j{}^2 = B_j{}^2 + R_j{}^2 \tag{15}$$

where the subscript j represents one of the parameters in Eq. (12). The total uncertainty of a particular parameter is composed of two parts, the systematic or bias uncertainty (B_j) and the precision or random uncertainty (R_j). In general, the bias uncertainty is contained in the measurement equipment and can be reduced, e.g. by using different equipment; the random uncertainty is inherent in any measured process and cannot be reduced by experimental techniques. The bias and precision uncertainties for each parameter will be discussed in the following.

1.8.1 Uncertainty in Initial Temperature

The bias uncertainty in the initial temperature is due to the standard limits of error of the K-type thermocouple used to measure the initial temperature. According to the Omega Engineering specifications, this is "the greater of 2.2 °C or 0.75%". The largest initial temperature used in this work, 413 K, leads to an uncertainty of 3 K; thus, $B_{T_O} = 3$ K. Bias uncertainty due to the A/D converter in the process meter is negligible compared to this uncertainty. The precision uncertainty is due to the limit of precision of the display on the Omega Engineering CNi3254 process meter used to control the process temperature. This is 0.05 K. The total uncertainty of the initial temperature is

$$U_{T_0} = \sqrt{\left(B_{T_0}\right)^2 + \left(R_{T_0}\right)^2} = \sqrt{(3\,\mathrm{K})^2 + (0.05\,\mathrm{K})^2} = 3\,\mathrm{K} \tag{16}$$

1.8.2 Uncertainty in Initial Pressure

The bias uncertainty in the initial pressure is due to the standard error in the pressure transducer used to measure the initial pressure. Two different pressure transducers have been used in this study; the first, an Omega Engineering PX-303 (range: 0–50 psia), has a full scale uncertainty of 1.25%, or 0.625 psi (4309.2 Pa). The second transducer is an Omega Engineering MMA100V10T2D0T4A6 type (range: 0–5200 Torr) and was purchased because preliminary results of this uncertainty analysis indicated that the largest contributor to the uncertainty of T_C was the initial pressure measurement. The full scale uncertainty of the MMA type transducers is 0.05%, resulting in an uncertainty of 2.6 Torr (346.6 Pa), an order of magnitude lower than the PX-303 while also providing more than double the operating range. Total uncertainties using the appropriate pressure transducer are reported in each experimental section of this work; both transducers will be analyzed in this section. Bias uncertainty due to the signal acquisition equipment is negligible compared to the standard error in the pressure transducers.

The precision uncertainty is due to the limit of precision of the display on the Omega Engineering DP41-B process meter used to monitor the initial pressure. This is 0.005 Torr (0.666 Pa). The

total uncertainty of the initial pressure is

$$U_{P_0} = \sqrt{\left(B_{P_0}\right)^2 + \left(R_{P_0}\right)^2} = \sqrt{(4309.2\,\text{Pa})^2 + (0.666\,\text{Pa})^2} = 4309.2\,\text{Pa} \tag{17a}$$

$$U_{P_0} = \sqrt{\left(B_{P_0}\right)^2 + \left(R_{P_0}\right)^2} = \sqrt{(346.6\,\text{Pa})^2 + (0.666\,\text{Pa})^2} = 346.6\,\text{Pa} \tag{17b}$$

1.8.3 Uncertainty in Compressed Pressure

The bias uncertainty in the compressed pressure is due to the standard error in the piezoelectric pressure transducer. According to the manufacturer's calibration, the deviation of the full scale output from linearity is less then 0.2%, indicating that $B_{T_C} = 0.5\,\text{bar}$. The uncertainties in the signal acquisition equipment are negligible compared to this uncertainty. The precision uncertainty is due to the limit of precision of the output of the pressure, and is 5×10^{-7} bar. This is negligible compared to the bias uncertainty, so the total uncertainty of the compressed pressure is

$$U_{P_C} = B_{T_C} = 0.5\,\text{bar} \tag{18}$$

1.8.4 Uncertainty in the Specific Heat

The uncertainty in the specific heat comes from two sources. First is the uncertainty in the mixture composition and second is the uncertainty in the linear fit to the total specific heat. The uncertainty in the mixture composition can be estimated by the same method as is used for T_C. The specific heat is given by Eq. (8), so we can take partial derivatives of that equation with respect to the mole fractions of the species to find the total uncertainty

$$\begin{aligned}\left(U_{\hat{C}_{p,\text{total}}}\right)^2 &= \left(\frac{\partial \hat{C}_p}{\partial X_1} U_{X_1}\right)^2 + \ldots + \left(\frac{\partial \hat{C}_p}{\partial X_n} U_{X_n}\right)^2 \\ &= \left(\hat{C}_{p,1} U_{X_1}\right)^2 + \ldots + \left(\hat{C}_{p,n} U_{X_n}\right)^2\end{aligned} \tag{19}$$

where n is the total number of species. In Eq. (19), it is assumed that the uncertainty in the specific heats of each species is negligible. This is considered an acceptable assumption for stable species

such as the fuel molecules, oxygen, nitrogen, and argon. Experience with several kinetic mechanisms has shown that the typical variation in individual $\hat{C}_p$ fits causes approximately 1 K changes in T_C.

The uncertainty of the mole fraction of the species is estimated differently depending on how the species was introduced to the mixing tank. For liquid fuel species, experiments with GC/MS have shown that there is approximately 5% variation in mole fraction from the expected value [20]; this value is adopted for the total uncertainty of all liquid fuels. The mole fraction of the gaseous species is determined by their partial pressures when filling; the mole fraction is related to the pressure by Dalton's Law of Partial Pressure [27, 28]

$$X_i = \frac{P_i}{P} \tag{20}$$

where P_i is the partial pressure of a species and P is the total pressure. It follows that

$$\begin{aligned} \left(U_{X_i}\right)^2 &= \left(\frac{\partial X_i}{\partial P_i} U_{P_i}\right)^2 + \left(\frac{\partial X_i}{\partial P} U_P\right)^2 \\ &= \left(\frac{U_{P_i}}{P}\right)^2 + \left(\frac{-P_i}{P^2} U_P\right)^2 \end{aligned} \tag{21}$$

The uncertainties of the pressures P_i and P are equal and can be estimated by the same procedure as in Sec. 1.8.2 since the same pressure transducer is used to measure the pressure. The total pressure P will be different for each species as it is filled. The order followed in these experiments is liquid fuel injection, followed by oxygen, then nitrogen, then argon; for propene, the order is oxygen, nitrogen, argon, propene.

A typical total pressure after filling is approximately 1300 Torr (≈ 173,319 Pa). The mixtures in Table 1 are the mixtures that will be analyzed in the following because they represent a worst case scenario in that the mole fraction of the fuel or oxygen is maximized in them.

Once the total specific heat has been calculated, a linear fit as a function of temperature is applied by least-squares estimation. Since there is an uncertainty in the specific heat, there is a

Table 1: Mixtures studied in the uncertainty analysis.

Fuel	Mole Fraction			
	Fuel	Oxygen	Nitrogen	Ar
Methylcyclohexane	0.0107	0.2240	0.0000	0.7653
n-Butanol	0.0676	0.2030	0.7294	0.0000
i-Pentanol	0.0531	0.1989	0.7480	0.0000
Propene	0.0854	0.1921	0.7225	0.0000

corresponding uncertainty in the fit coefficients a and b. Following the methodology outlined by York et al. [29], the values and uncertainties of a and b are calculated iteratively. This procedure gives identical values of the slope, intercept, and standard errors as maximum likelihood estimation [29]. Equation 22 is reproduced from York et al. [29], and is presented as Eq. (13) in that work.

$$a = \overline{Y} - b\overline{X} \tag{22a}$$

$$b = \frac{\sum W_i \beta_i V_i}{\sum W_i \beta_i U_i} \tag{22b}$$

$$\sigma_a^2 = \frac{1}{\sum W_i} + \overline{x}^2 \sigma_b^2 \tag{22c}$$

$$\sigma_b^2 = \frac{1}{\sum W_i u_i^2} \tag{22d}$$

where the symbols in Eq. (22) are defined in Table 2. The general formulation is given here because it will be reused in **??**; application to this section will be given below.

In this section, X_i are the temperatures at which Eq. (10) is evaluated and Y_i are the total specific heats evaluated from Eq. (10). The weighting of the specific heats—$\omega(Y_i)$—is taken to be the reciprocal of the uncertainty as calculated by Eq. (19). Furthermore, there is no uncertainty in the abscissa (i.e. the temperature) and $\omega(X_i) = 1$. Finally, since there is no uncertainty in the temperature, there is no correlation between the uncertainties, i.e. $r_i = 0$.

First, the slope b is estimated by simple least-squares regression of the total specific heat on the temperature. Then, this slope is used to estimate the adjusted weighting of each point, W_i. Next, U_i and V_i are calculated based on the adjusted weighting. Using U_i, V_i, and β_i, a new value of the slope is calculated from Eq. (22b), and the process is repeated until the slope converges. Convergence

Table 2: Symbols in Eq. (22). Reproduced from the work of York et al. [29].

Symbol	Meaning
a, b	y intercept and slope of best line, $y = a + bx$
σ_a, σ_b	Standard errors of a and b
X_i, Y_i	"Observed" data points
r_i	Correlation coefficient between uncertainty in X_i and Y_i
$\omega(X_i), \omega(Y_i)$	Weights of X_i and Y_i
x_i, y_i	$\overline{X} + \beta_i, \overline{Y} + b\beta_i$
α_i	$\sqrt{\omega(X_i)\omega(Y_i)}$
W_i	$\dfrac{\omega(X_i)\omega(Y_i)}{\omega(X_i) + b^2\omega(Y_i) - 2r_i\alpha_i b}$
$\overline{X}, \overline{Y}$	$\dfrac{\sum W_i X_i}{\sum W_i}, \dfrac{\sum W_i Y_i}{\sum W_i}$
U_i, V_i	$X_i - \overline{X}, Y_i - \overline{Y}$
$\overline{x}$	$\dfrac{\sum W_i x_i}{\sum W_i}$
β_i	$W_i\left[\dfrac{U_i}{\omega(Y_i)} + \dfrac{bV_i}{\omega(X_i)} - (bU_i + V_i)\dfrac{r_i}{\alpha_i}\right]$
u_i	$x_i - \overline{x}$

is determined when the slope changes by less than 0.001 on successive iterations. Then, using Eq. (22a), the intercept a is calculated. Finally, the standard error of each parameter is calculated using the final values of the slope and intercept with Eqs. (22d) and (22c).

For the mixtures considered in this study, the correlation coefficient for the linear fits are greater than 0.99 (i.e. $r^2 > 0.99$), indicating a good fit.